

PAPER • **OPEN ACCESS**

## Distinct antiblockade features of strongly interacting Rydberg atoms under a two-color weak excitation scheme

To cite this article: Suying Bai *et al* 2020 *New J. Phys.* **22** 013004

View the [article online](#) for updates and enhancements.



## OPEN ACCESS

## RECEIVED

30 September 2019

## REVISED

22 December 2019

## ACCEPTED FOR PUBLICATION

24 December 2019

## PUBLISHED

14 January 2020


Original content from this work may be used under the terms of the [Creative Commons Attribution 3.0 licence](#).

Any further distribution of this work must maintain attribution to the author(s) and the title of the work, journal citation and DOI.



## PAPER

## Distinct antiblockade features of strongly interacting Rydberg atoms under a two-color weak excitation scheme

Suying Bai<sup>1,4</sup>, Xuedong Tian<sup>2</sup>, Xiaoxuan Han<sup>1,4</sup>, Yuechun Jiao<sup>1,4</sup>, Jinhui Wu<sup>3</sup>, Jianming Zhao<sup>1,4</sup>  and Suotang Jia<sup>1,4</sup><sup>1</sup> State Key Laboratory of Quantum Optics and Quantum Optics Devices, Institute of Laser Spectroscopy, Shanxi University, Taiyuan 030006, People's Republic of China<sup>2</sup> College of Physics Science and Technology, Guangxi Normal University, Guilin 541004, People's Republic of China<sup>3</sup> School of Physics, Northeast Normal University, Changchun 130024, People's Republic of China<sup>4</sup> Collaborative Innovation Center of Extreme Optics, Shanxi University, Taiyuan 030006, People's Republic of China**Keywords:** antiblockade, dynamic evolution, multilevel two-body model

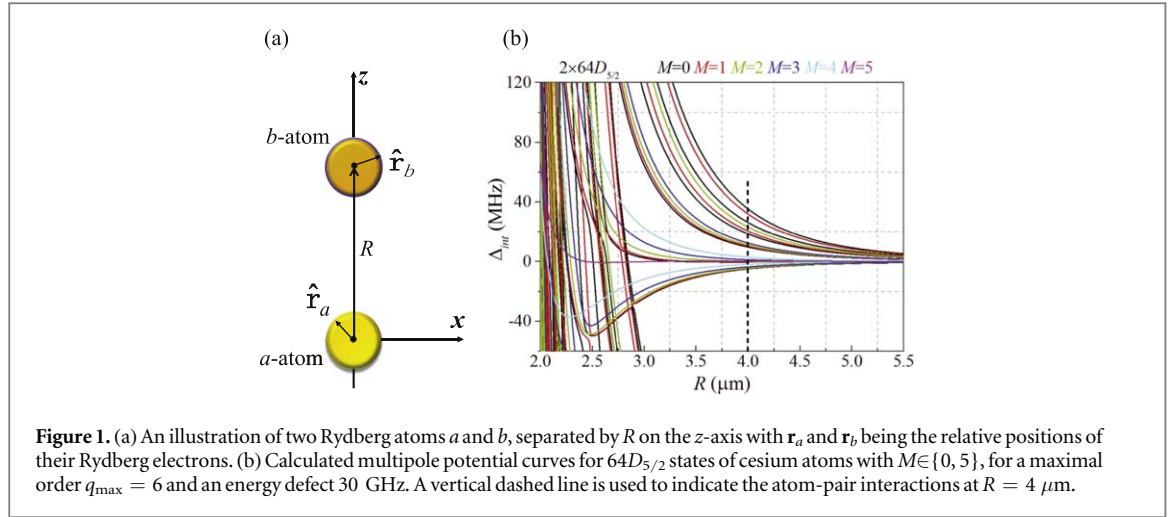
## Abstract

We present distinct antiblockade features of strongly interacting  $64D_{5/2}$  Rydberg atoms employing a two-color excitation scheme. The first color (pulse A) is set to resonantly excite a few seed Rydberg atoms, each of which establishes a blockade region due to the long-range multipole interactions. The second color (pulse B) is blue detuned so that the multipole-interaction-induced shifts of certain atoms are well compensated to result in the antiblockade effect. We find in particular that a few seed atoms can lead to a remarkable difference of the Rydberg excitation in the presence of pulse B for a wide range of blue detuning. Relevant dynamics of this antiblockade excitation is also investigated by varying the pulse-B duration for a fixed blue detuning, further confirming the facilitation process of Rydberg excitation accompanied by a saturation effect. These experimental results can be well recovered by theoretical simulations based on a multilevel two-body model.

## 1. Introduction

Creating ultracold gases in the  $\mu\text{K}$  regime has opened a new avenue for the investigation of strongly interacting systems. For nondegenerate gases in a magneto-optical trap (MOT), the interaction between ground state atoms is typically very weak. However, Rydberg atoms with principal quantum numbers  $n \gtrsim 10$  can strongly interact, even in a dilute gas, due to their long-range dipole-dipole ( $\sim n^4$ ) and Van der Waals (vdw) interactions ( $\sim n^{11}$ ) [1]. These scalings allow for accurately controlling the interactions over a large range by varying  $n$ . The strong interaction between Rydberg atoms shifts the energy level and suppresses the further excitation of nearby atoms, leading to a blockade effect [2, 3]. The blockade radius  $R_B$  is usually defined as the distance between two atoms at which the interaction-induced shift equals the excitation linewidth. Within the region of  $R < R_B$ , only one Rydberg atom can be excited, yielding thus the blockade volume of a single Rydberg excitation. In this case, a superatom is formed as the superposition of one Rydberg atom and many ground-state atoms [4, 5]. Based on the blockade effect, Rydberg atoms can be employed to implement quantum information processing [6, 7], quantum registers [8–11], single-photon sources [12, 13] and transistors [14–16]. Rydberg atoms are also an ideal platform for investigating excitation transfer [17–20] and many-body dynamics [21] and implementation of atomic arrays [22, 23] beyond the blockade regime.

But we note that it is also viable to have two or more Rydberg atoms in a blockade region under appropriate driving schemes. This so-called antiblockade effect has been investigated by several groups to consider different topics. In particular, the evidence of antiblockade has been observed as an asymmetric Autler–Townes structure when cold rubidium atoms are modeled by a three-level system with the lower transition resonantly driven by a strong laser [24, 25]. The antiblockade effect may also manifest itself in enhanced excitation probabilities only on the blue side of resonance when full counting statistics is investigated for an effective two-level model of cold Rydberg atoms [26, 27]. Dynamics of the aggregation or facilitation process is further verified as a result of the successive antiblockade excitation of  $nS$  states in room-temperature gases with a strong inhomogeneous



broadening [28, 29]. Meanwhile similar seeded excitation avalanches of 70S cold atoms have been experimentally observed in an off-resonantly driving scheme and theoretically simulated with a simple bimodal approach [30]. It is thus of interest to explore the facilitated antiblockade excitation of high-angular-momentum, e.g.  $nD$ , states by adopting suitable driving schemes.

Different from previous works [24–30], here we study the long-range multipole interaction between  $64D_{5/2}$ -atom pairs by focusing on the antiblockade effect in a dilute sample of cold cesium atoms. A largely enhanced Rydberg excitation is realized by a two-color double-resonance method, in which pulse-A excites resonantly a few seed atoms whereas the frequency of pulse-B is detuned to compensate the multipole-interaction-induced shift of nearby atoms. The antiblockade effect now features as a *long tail* of the enhanced Rydberg excitation on the blue side of resonance. This is attained in the *nontrivial* regime where the Rabi frequency of pulse-B is too small to compensate its detuning (comparable to long-range interaction) so that the Rydberg excitation is negligible in the absence of pulse-A. Evolution dynamics is also measured by varying the duration of pulse-B, further showing an aggregation-like saturation effect of the Rydberg excitation. A multilevel two-body model has been developed to simulate the facilitated antiblockade excitation of  $D$ -type Rydberg atoms with many magnetic sublevels.

## 2. Long-range interaction model

We now briefly introduce the theoretical model for calculating the multipole interaction potential of  $nD_J$  Rydberg states, while details can be found in our previous works [31, 32]. As shown in figure 1(a), for two  $nD_J$  Rydberg atoms, denoted by  $a$  and  $b$ , with an interatomic separation  $\mathbf{R}$  along the quantization  $z$ -axis, we first assume that (i) their Rydberg electrons have positions  $\mathbf{r}_a$  and  $\mathbf{r}_b$  and (ii) the interatomic distance  $R$  is larger than the LeRoy radius  $R_{\text{LR}}$  [33]. Then the Hamiltonian for such a pair of Rydberg atoms can be written as

$$\hat{H} = \hat{H}_a + \hat{H}_b + \hat{V}_{\text{int}}, \quad (1)$$

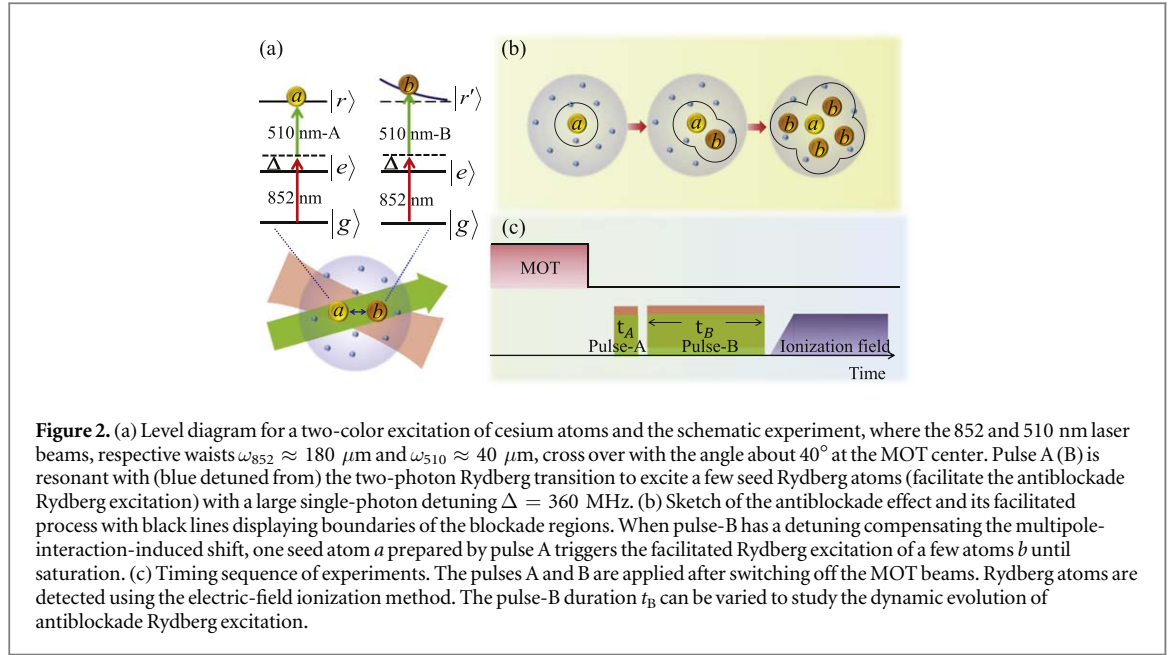
where  $\hat{H}_{a(b)}$  is the Hamiltonian of atom  $a(b)$ , and  $\hat{V}_{\text{int}}$  denotes the multipole interaction [31, 32, 34, 35]

$$\hat{V}_{\text{int}} = \sum_{q=2}^{q_{\max}} \frac{1}{R^{q+1}} \sum_{L_a=1, L_b=q-L_a}^{q_{\max}-1} \sum_{\Omega=-L_<}^{L_<} f_{ab\Omega} \hat{Q}_a \hat{Q}_b, \quad (2)$$

$$f_{ab\Omega} = \frac{(-1)^{L_b} (L_a + L_b)!}{\sqrt{(L_a + \Omega)!(L_a - \Omega)!(L_b + \Omega)!(L_b - \Omega)!}}, \quad (3)$$

where  $L_{a(b)}$  is the multipole order of atom  $a(b)$ , and  $L_<$  is the lesser of  $L_a$  and  $L_b$ . The sum over  $q = L_a + L_b$  starts at 2 (because atoms are neutral and have no monopole moment) and is truncated at a maximal order  $q_{\max}$ . The factor  $f_{ab\Omega}$  depends on the multipole orders  $L_a$  and  $L_b$  and the counting index  $\Omega$  in the third sum. The operators  $\hat{Q}_{a(b)} = \sqrt{\frac{4\pi}{2L_{a(b)}+1}} \hat{r}_{a(b)}^{L_{a(b)}} Y_{L_{a(b)}}^{\Omega}(\hat{\mathbf{r}}_{a(b)})$  include the radial matrix elements  $\hat{r}_{a(b)}^{L_{a(b)}}$  and the angular-dependent spherical harmonics  $Y_{L_{a(b)}}^{\pm\Omega}(\hat{\mathbf{r}}_{a(b)})$ .

We then diagonalize the Hamiltonian of the Rydberg-atom pair on a dense grid of  $R$  in the  $\{2.0, 5.5\} \mu\text{m}$  range with 400 steps. To improve the plot quality of the potential curves at small  $R$ , the radial steps have been chosen equidistant in  $R^{-3}$ . Because of global azimuthal symmetry, the projection of the sum of the electronic angular momenta,  $M = m_{Ja} + m_{Jb}$ , is conserved. In figure 1(b), we present the calculated interaction potential



curves by considering (i) the single-atom orbital angular momentum (magnetic quantum number)  $\ell \leq \ell_{\max}$  ( $m_J \leq m_{J\max}$ ); (ii) the energy defect 30 GHz of two-body states; (iii) the range of effective principal quantum numbers  $\text{int}(n_{\text{eff0}}) - \delta < n_{\text{eff}} < \text{int}(n_{\text{eff0}}) + \delta + 1$ , with  $\text{int}(n_{\text{eff0}})$  denoting the integer part of  $n_{\text{eff0}}$  and  $\delta$  being a parameter determining the range of  $n_{\text{eff}}$ .

For all molecular states corresponding to a fixed value of  $M$  shown in figure 1(a), only one potential curve exhibits a minimum that could give rise to a bound Rydberg macrodimer [31], while all other potential curves just exhibit the repulsive interactions. For the typical atomic density  $N \sim 10^{10} \text{ cm}^{-3}$  in a MOT, we have the average interatomic separation  $R \sim 4.0 \mu\text{m}$ , marked by a dashed line in figure 1(b), and thus the repulsive interaction  $\Delta_{\text{int}} = \langle \hat{V}_{\text{int}} \rangle = 2\pi \times 5 \sim 40 \text{ MHz}$  for a Rydberg pair in the  $64D_{5/2}$  state. It is this strong long-range repulsive interaction that leads to the blockade effect. In the following section, we focus on the blue-detuned side of the  $64D_{5/2}$  atomic resonance and investigate the facilitated antiblockade effect in a two-color excitation scheme.

### 3. Experimental setup

Our antiblockade experiments are performed in a standard cesium MOT, the atomic cloud has a diameter  $\sim 600 \mu\text{m}$ , density  $\sim 3 \times 10^{10} \text{ cm}^{-3}$  and temperature  $\sim 100 \mu\text{K}$ , measured by a shadow imaging technique. After switching off the MOT beams, we successively switch on a resonant pulse A and a detuned pulse B in the timing sequence as sketched in figure 2(c). Both pulses are applied in the two-photon excitation scheme (see figure 2(a)) by stabilizing a ‘Toptica DLpro’ laser (852 nm wavelength and 100 kHz linewidth) to the  $|6S_{1/2}, F = 4\rangle (|g\rangle) \rightarrow |6P_{3/2}, F' = 5\rangle (|e\rangle)$  lower transition via a polarization spectroscopy technique [36] and a ‘Toptica TA SHG110’ laser (510 nm wavelength and 1 MHz linewidth) to the  $|6P_{3/2}, F' = 5\rangle (|e\rangle) \rightarrow |64D_{5/2}\rangle (|r\rangle)$  upper transition with a F-P cavity of finesse 15000. The 852 nm laser has a fixed 360 MHz blue detuning relative to the lower transition for both pulse A and pulse B as controlled by a double-pass acousto-optic modulator (AOM). The 510 nm laser, however, is controlled by another AOM to attain the two-photon resonant (detuned) excitation of  $64D_{5/2}$  state for pulse A (pulse B). During the scan of two-photon detuning for pulse B, the laser power is held fixed using a PID (proportional integral derivative) feedback loop that controls the RF power supplied to the 510 nm AOM. To be more specific, the 852 and 510 nm lasers have powers  $\sim 270 \mu\text{W}$  and  $\sim 13.3 \text{ mW}$ , respectively, corresponding to single-photon Rabi frequencies  $\Omega_{852} = 2\pi \times 48.5 \text{ MHz}$  on the lower transition and  $\Omega_{510} = 2\pi \times 6.4 \text{ MHz}$  on the upper transition. Then it is easy to get the two-photon effective Rabi frequency  $\Omega_{\text{eff}} = 2\pi \times 0.43 \text{ MHz}$ , which will be used for theoretical simulations in section 5.

The 852 nm and 510 nm laser beams of waists  $180 \mu\text{m}$  and  $40 \mu\text{m}$ , respectively, cross over with an angle about  $40^\circ$  at the MOT center, yielding thus an elliptical excitation region. This cross-beam scheme allows the atomic density within the excitation region to maintain nearly identical. The excitation region is surrounded by three pairs of field-compensation electrodes so that stray electric fields can be reduced to less than  $50 \text{ mV cm}^{-1}$  via the Stark spectroscopy. Rydberg atoms are detected using a ramp ionization field (ramp time  $\approx 3 \mu\text{s}$ ), which is

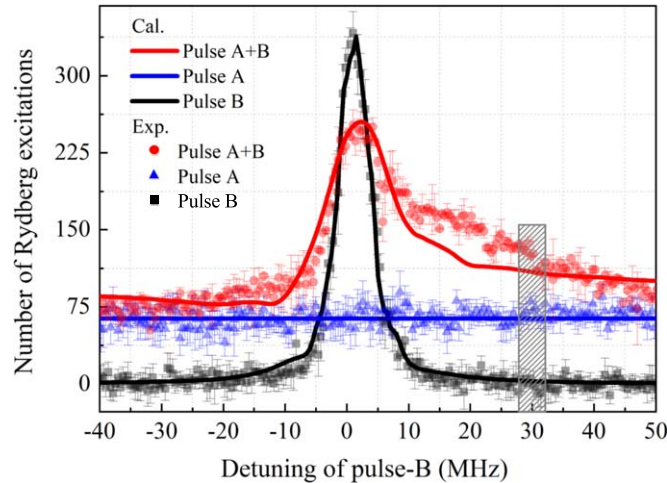


**Figure 3.** Measurements (samples) and calculations (lines) of the Rydberg excitation versus the detuning of pulse B for switching on only pulse A (blue triangles), only pulse B (black squares) and both pulses (red circles). With only pulse A, the number of Rydberg excitations remains unchanged because the detuning of pulse B is meaningless. With only pulse B, the number of Rydberg excitations is largely enhanced when pulse B is scanned through the two-photon Rydberg transition. When both pulses are applied, the Rydberg excitation is suppressed at two-photon resonance but facilitated in a wide range of blue detuning of pulse B. A gray square denotes the 30 MHz detuning, where the number of Rydberg excitations is about 2 times as that observed with only pulse A. The measured number of Rydberg excitations is corrected for the detection efficiency and the calculations are multiplied by a factor of 3.8.

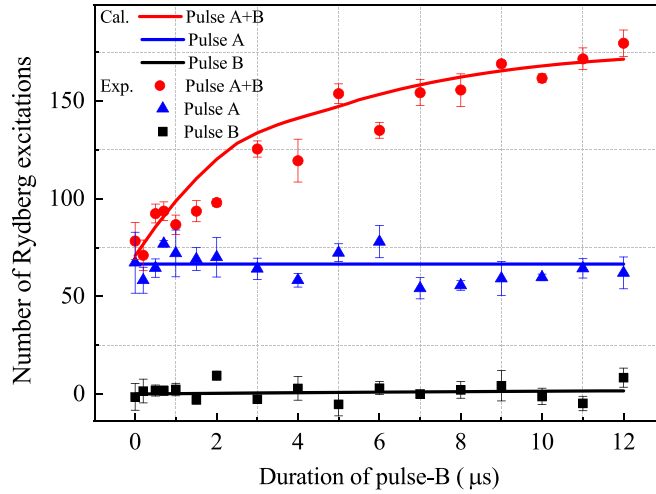
large enough to ionize all Rydberg atoms in  $64D_{5/2}$  and nearby states transferred due to blackbody radiation. The Rydberg ions are detected with a microchannel plate (MCP) detector, which has detection efficiency of about 20%. The detected ion signals are amplified with an amplifier and analyzed with a boxcar integrator (SRS-250) and then recorded with a computer. Before the measurements, we first calibrate the MCP ions detection system with two shadow images taken before and after the laser excitation. From the difference of two shadow images, we can obtain the number of Rydberg excitations and therefore the gain factor  $f_{\text{gain}}$  of the MCP detection system,  $f_{\text{gain}} \approx 3.67$  mV in this work. The actual number of Rydberg excitations will be taken as  $R_{\text{sig}}/f_{\text{gain}}$  ( $R_{\text{sig}}$  is the measured Rydberg signal).

Figure 2(b) shows the basic idea of our antiblockade excitation scheme. Once pulse A resonantly excites a Rydberg-atom  $a$ , its neighbor atoms in the blockade region, black line in the left part of figure 2(b), will undergo level shifts due to strong Rydberg interactions as shown in figure 1(b). The subsequent detuned pulse B results in the resonant Rydberg excitation restricted to specific distances and therefore the formation of so-called antiblockade or the facilitated excitation. The facilitated excitation mainly occurs at the boundary of a blockade region, denoted with  $b$  in the middle part of figure 2(b). The Rydberg atom  $b$  is thought as a new seed atom that expands the blockade region and leads to an aggregation process of Rydberg excitation. The number of Rydberg excitations increases during the aggregation process and saturates after a certain time, as shown in the right part of figure 2(b).

#### 4. Experimental observation of antiblockade

We first study how a few seed atoms excited by pulse A affect the Rydberg excitation due to pulse B. We consider three cases where only pulse A, only pulse B, or both pulses are switched on. Figure 3 presents the Rydberg excitation spectra as a function of pulse B detuning when pulse A and pulse B have the  $0.4 \mu\text{s}$  and  $6.0 \mu\text{s}$  durations, respectively. It is clear that pulse A itself prepares a few seed Rydberg atoms, whose number is small and keeps unchanged as we scan the pulse-B detuning. Pulse-B itself results in a 5 times larger signal of Rydberg excitation at the zero detuning, and the signal exhibits a Lorentzian profile of linewidth  $\approx 8$  MHz. Outside this Lorentzian profile, no atoms can be excited to the Rydberg state when only pulse B is applied.

However, if we apply a  $0.4 \mu\text{s}$  pulse A before pulse B, the Rydberg excitation process becomes very different. That is, the Rydberg excitation is slightly suppressed at resonance,  $\sim 20\%$  less than that with only pulse B, due to the blockade effect of pulse A. It is interesting that the Rydberg excitation is largely enhanced in a wide range (10–50 MHz here) of blue detuning due to the facilitated antiblockade effect. To be more specific, the Rydberg excitation is vanishing at the 20 MHz blue detuning when only pulse B is applied, but is clearly enhanced by a factor of 2.5 when pulse A is applied before pulse B. At the 30 MHz blue detuning, as marked with the gray squares, the enhanced Rydberg excitation is less than that at the 20 MHz blue detuning with an enhanced factor



**Figure 4.** Measurements (samples) and simulations (lines) of the Rydberg excitation as a function of the pulse B duration when pulse B has a 30 MHz blue detuning and pulse A is resonant to the Rydberg transition. Once again we consider three cases where only pulse A (blue triangles), only pulse B (black squares), or both pulses (red circles) are switched on. The increase of pulse B duration does not affect the number of Rydberg excitation in the case of only switching on pulse A or B, but results in a nonlinear increase of the number of Rydberg excitations in the case of switching on both pulses. The measured number of Rydberg excitations is corrected for the detection efficiency and the calculations are multiplied by a factor of 3.8.

of 2 instead. The large difference between the three curves demonstrates that the existence of a small amount of seed atoms  $a$  greatly facilitates the excitation probability of pulse B at the blue detuned side.

Note, however, that the Rydberg excitation also shows the antiblockade effect at the red detuned side. But the increased excitation is much weaker, e.g. at the  $-10$  MHz position, than that at the blue detuned side. This is because only one potential curve shows attractive interaction for every molecule state  $M$ , whose strength is much less than the repulsive interactions as shown in figure 1(b). A Rydberg molecular signal will be obtained at the pulse B detuning  $\sim 50$  MHz, which is beyond the scope of this work (see [31, 32] for details) and thus not shown.

To gain a deeper insight into the Rydberg facilitation process, we have also done a series of dynamic measurements on the Rydberg excitation by varying the pulse-B duration while keeping the zero (30 MHz) detuning for pulse A (B), as shown in figure 4. In the case where only pulse A or B is turned on, the Rydberg population does not change when the pulse-B duration increases, as denoted by blue triangles (only pulse A) and black squares (only pulse B). This is because the Rydberg excitation due to pulse A is irrelevant to the pulse-B duration in the absence of pulse B, and pulse B excites nothing as it is far detuned from the Rydberg transition in the absence of seed Rydberg atoms. But when both pulses are turned on, as denoted by red circles, the Rydberg excitation demonstrates completely different characteristics. That is, the number of Rydberg excitation first quickly increases when the pulse-B duration is increased until  $5 \mu\text{s}$  and then gradually approaches a saturation value.

We also note that initially prepared Rydberg population in  $64D_{5/2}$  can be redistributed to nearby dipole allowed levels by blackbody radiation [37]. The time-of-flight spectra in our experiments prominently demonstrate the excitation of  $64D_{5/2}$  state while a small fraction of the signal can be attributed to the nearby  $P$  states when pulse B has a duration  $> 6 \mu\text{s}$ . Meanwhile, for a short pulse-A duration and a small number of  $64D_{5/2}$  atoms, we do not see any free-ion signals due to the redistribution of initially prepared Rydberg atoms [37]. So the  $P$ -state signals induced by the blackbody radiation can be neglected in our work.

## 5. Simulations based on multilevel two-body model

We now try to simulate the above experimental observations with a multilevel two-body theoretical model [38] by including different multipole-interaction-induced shifts of all magnetic sublevels of the Rydberg state based on the following two considerations. First, the lower (852 nm) and upper (510 nm) excitation lasers have Rabi frequencies  $\Omega_{852}^j = 2\pi \times 48.5$  MHz,  $\Omega_{510}^j = 2\pi \times 6.4$  MHz, and single-photon detuning  $\Delta = \Delta_{852}^j \approx -\Delta_{510}^j \approx 2\pi \times 360$  MHz for pulse  $j \in \{A, B\}$  as taken from the experiment, so we can eliminate level  $|e\rangle$  to have an effective Rabi frequency  $\Omega_{\text{eff}}^j = \Omega_{852}^j \Omega_{510}^j / 2\Delta^j \approx 2\pi \times 0.43$  MHz that couples levels  $|g\rangle$  and  $|r\rangle$ . Second, the average atomic distance is  $R \sim 4.0 \mu\text{m}$  from the averaged atomic density  $N \sim 10^{10} \text{ cm}^{-3}$ , so we know from figure 1(b) that the multipole interaction between two nearest-neighbor (next-nearest-neighbor) atoms is much stronger (smaller) than  $\Omega_{\text{eff}}^a$ . Then, roughly two atoms can be found in each blockade volume so that we just need to consider the multipole



interactions of atomic pairs. Aiming to attain more accurate results, however, we write down the effective Hamiltonian without neglecting level  $|e\rangle$

$$H_{\text{eff}}^j = \sum_{i=a,b} [\Delta_{852}^j |e_i\rangle \langle e_i| + (\Delta_{852}^j + \Delta_{510}^j) |r_i\rangle \langle r_i|] + \Delta_{\text{int}} |r_a r_b\rangle \langle r_b r_a| \\ + \sum_{i=a,b} [\Omega_{852}^j |e_i\rangle \langle g_i| + \Omega_{510}^j |r_i\rangle \langle e_i| + \Omega_{852}^j |g_i\rangle \langle e_i| + \Omega_{510}^j |e_i\rangle \langle r_i|],$$

for atoms  $a$  and  $b$  in each blockade volume ( $\hbar = 1$ ).

Taking  $H_{\text{eff}}^j$  into master equation  $\partial_t \rho^j = -i[H_{\text{eff}}^j, \rho^j]$  of density operator  $\rho^j$  and adding the decay ( $\Gamma_{\mu\nu}$ ) and dephasing ( $\gamma_{\mu\nu}$ ) rates, we obtain a set of dynamical equations for  $9 \times 9$  density matrix elements  $\rho_{\mu\nu,\mu\nu}^j$  with the former (latter)  $\mu$  and  $\nu$  referring to the three levels of atom  $a$  ( $b$ ) in the excitation process of pulses  $j$ . Then we use this set of equations to simulate the pulse A (B) excitation process by applying the resonant (detuned) pulse A (B) with  $\Delta_{\text{int}} = \{-4.0 \sim 34.0\} \times 2\pi$  MHz, taken from figure 1(b), for 21 interaction potentials formed with different magnetic sublevels with  $M \in \{0, 1, 2, 3, 4, 5\}$  of weight factor  $\zeta \in \{6, 5, 4, 3, 2, 1\}$ . We further note that (i) pulse A has a fixed duration  $t_A = 0.4 \mu\text{s}$  while the duration  $t_B$  for pulse B will be varied in the range  $\{0 \sim 12\} \mu\text{s}$  in our simulations; (ii) our numerical results are attained as a sum of 21 independent numerical realizations with different magnetic sublevels serving as level  $|r_i\rangle$ ; (iii) the resonant A excitation process will result in a blockade effect while the off-resonant B excitation process is expected to yield an antiblockade effect.

Numerical simulations on the excitation spectra are displayed with solid lines in figure 3 under three indicated conditions with regard to the application of pulse-A and pulse-B. It is seen that our calculations can well reproduce the experimental results when only pulse-A or pulse-B is switched on. Whereas in the case where both pulses are applied, the calculated spectrum is just basically consistent with its experimental counterpart. To be more concrete, our calculations seem to slightly underestimate the experimental results around  $-10$  MHz and  $20$  MHz detuning. This may be attributed to the fact that we have assumed for simplicity the seed Rydberg atoms excited by pulse-A have a homogeneous distribution in the whole sample. In figure 4, we further simulate the Rydberg excitation dynamics when pulse-B is fixed at  $30$  MHz detuning, marked with the gray square in figure 3. Our calculations well reproduce the experimental results in all three cases, consistent with corresponding steady-state results in figure 3. In particular, we find that the Rydberg excitation tends to a saturation value with numerical calculations and experimental results being more consistent when pulse-B has a long enough duration (e.g. for  $t_B > 8 \mu\text{s}$ ). This means that the assumption of homogeneously distributed seed Rydberg atoms is more reasonable for a more persistent excitation due to pulse-B. Finally, we note that the calculations in figures 3 and 4 display in fact the two-color excitation probabilities, which have been multiplied by a factor of 3.8 so that they could be quantitatively consistent with relevant experimental results.

## 6. Conclusions

In summary, we have investigated the long-range multipole interactions of cesium atoms in the  $64D_{5/2}$  state based on a two-color excitation scheme. The first color (pulse-A) is resonant with the Rydberg transition for preparing a few seed atoms in the blockade regime. The second color (pulse-B) is blue detuned from the Rydberg resonance for facilitating the antiblockade excitation. The two-color excitation scheme is found to work well for manipulating the antiblockade and facilitation processes of  $64D_{5/2}$  Rydberg state. That is, pulse-B excites atoms from the ground state to the Rydberg state only on resonance without the seed atoms, but enables the characterization of facilitation effect over a wide blue detuned range in the presence of seed atoms. We also measured the evolution dynamics of the Rydberg excitation and further found an aggregation-like saturation effect, which has been discussed in [30] for  $70S$  Rydberg state of rubidium atoms. To understand the experimental observations, we have developed a multilevel two-body model by including multipole-interaction-induced shifts for all magnetic sublevels of different excitation weights. The simulations reproduce successfully the measurements on both excitation spectra and dynamic evolutions.

## Acknowledgments

We thank G Raithel for discussions on the calculation of multipole Rydberg potentials. The work was supported by the National Key R&D Program of China (Grant No. 2017YFA0304203), the National Natural Science Foundation of China (Grants Nos. 61675123, 61775124 and 11804202, 11847018), the State Key Program of National Natural Science of China (Grant No. 11434007 and 61835007), and Changjiang Scholars and Innovative Research Team in University of Ministry of Education of China (Grant No. IRT\_17R70).

## ORCID iDs

Jianming Zhao  <https://orcid.org/0000-0001-8420-9319>

## References

- [1] Gallagher T F 1994 *Rydberg Atoms* (Cambridge: Cambridge University Press)
- [2] Tong D, Farooqi S M, Stanojevic J, Krishnan S, Zhang Y P, Côté R, Eyler E E and Gould P L 2004 *Phys. Rev. Lett.* **93** 063001
- [3] Singer K, Reetz-Lamour M, Amthor T, Marcassa L G and Weidemüller M 2004 *Phys. Rev. Lett.* **93** 163001
- [4] Liu Y M, Yan D, Tian X D, Cui C L and Wu J H 2014 *Phys. Rev. A* **89** 033839
- [5] Petrosyan D, Otterbach J and Fleischhauer M 2011 *Phys. Rev. Lett.* **107** 213601
- [6] Saffman M, Walker T G and Mølmer K 2010 *Rev. Mod. Phys.* **82** 2313–63
- [7] Lukin M D, Fleischhauer M, Cote R, Duan L M, Jaksch D, Cirac J I and Zoller P 2001 *Phys. Rev. Lett.* **87** 037901
- [8] Endres M, Bernien H, Keesling A, Levine H, Anschuetz E R, Krajenbrink A, Senko C, Vuletic V, Greiner M and Lukin M D 2016 *Science* **354** 1024
- [9] Xia T, Lichtman M, Maller K, Carr A W, Piotrowicz M J, Isenhower L and Saffman M 2015 *Phys. Rev. Lett.* **114** 100503
- [10] Kim H, Lee W, Lee H G, Jo H, Song Y and Ahn J 2016 *Nat. Commun.* **7** 13317
- [11] Lester B J, Luick N, Kaufman A M, Reynolds C M and Regal C A 2015 *Phys. Rev. Lett.* **115** 073003
- [12] Dudin Y O and Kuzmich A 2012 *Science* **336** 887
- [13] Peyronel T, Firstenberg O, Liang Q Y, Hofferberth S, Gorshkov A V, Pohl T, Lukin M D and Vuletić V 2012 *Nature* **488** 57
- [14] Li W B, Viscor D, Hofferberth S and Lesanovsky I 2014 *Phys. Rev. Lett.* **112** 243601
- [15] Gorniaczyk H, Tresp C, Schmidt J, Fedder H and Hofferberth S 2014 *Phys. Rev. Lett.* **113** 053601
- [16] Tiarks D, Baur S, Schneider K, Dürr S and Rempe G 2014 *Phys. Rev. Lett.* **113** 053602
- [17] Günter G, Schempp H, Robert-de Saint-Vincent M, Gavryusev V, Helmrich S, Hofmann C S, Whitlock S and Weidemüller M 2013 *Science* **342** 954–6
- [18] Barredo D, Ravets S, Labuhn H, Béguin L, Vernier A, Nogrette F, Lahaye T and Browaeys A 2014 *Phys. Rev. Lett.* **112** 183002
- [19] Barredo D, Labuhn H, Ravets S, Lahaye T, Browaeys A and Adams C S 2015 *Phys. Rev. Lett.* **114** 113002
- [20] Maineult W, Pelle B, Faoro R, Arimondo E, Pillet P and Cheinet P 2016 *J. Phys. B: At. Mol. Opt. Phys.* **49** 214001
- [21] Ates C, Pohl T, Pattard T and Rost J M 2007 *Phys. Rev. A* **76** 013413
- [22] Barredo D, Lienhard V, Léséleuc S, Lahaye T and Browaeys A 2018 *Nature* **561** 79
- [23] Mello D O, Schäffner D, Werkmann J, Preuschoff T, Kohfahl L, Schlosser M and Birkel G 2019 *Phys. Rev. Lett.* **122** 203601
- [24] Ates C, Pohl T, Pattard T and Rost J M 2007 *Phys. Rev. Lett.* **98** 023002
- [25] Amthor T, Giese C, Hofmann C S and Weidemüller M 2010 *Phys. Rev. Lett.* **104** 013001
- [26] Schempp H et al 2014 *Phys. Rev. Lett.* **112** 013002
- [27] Malossi N, Valado M M, Scotto S, Huillery P, Pillet P, Ciampini D, Arimondo E and Morsch O 2014 *Phys. Rev. Lett.* **113** 023006
- [28] Urvoy A, Ripka F, Lesanovsky I, Booth D, Shaffer J P, Pfau T and Löw R 2015 *Phys. Rev. Lett.* **114** 203002
- [29] Letscher F, Thomas O, Niederprüm T, Ott H and Fleischhauer M 2017 *Phys. Rev. A* **95** 023410
- [30] Simonelli C, Valado M M, Masella G, Asteria L, Arimondo E, Ciampini D and Morsch O 2016 *J. Phys. B: At. Mol. Opt. Phys.* **49** 154002
- [31] Han X X, Bai S Y, Jiao Y C, Hao L P, Xue Y M, Zhao J M, Jia S T and Raithel G 2018 *Phys. Rev. A* **97** 031403
- [32] Han X X, Bai S Y, Jiao Y C, Raithel G, Zhao J M and Jia S T 2019 *J. Phys. B: At. Mol. Opt. Phys.* **52** 135102
- [33] Le Roy R J 1974 *Can. J. Phys.* **52** 246
- [34] Schwettmann A, Crawford J, Overstreet K R and Shaffer J P 2006 *Phys. Rev. A* **74** 020701
- [35] Deiglmayr J, Saßmannshausen H, Pillet P and Merkt F 2014 *Phys. Rev. Lett.* **113** 193001
- [36] Pearman C P, Adams C S, Cox S G, Griffin P F, Smith D A and Hughes I G 2002 *J. Phys. B: At. Mol. Opt. Phys.* **35** 5141
- [37] Caliri L L and Marcassa L G 2007 *Phys. Rev. A* **75** 066503
- [38] Kondo J M, Booth D, Gonçalves L F, Shaffer J P and Marcassa L G 2016 *Phys. Rev. A* **93** 012703